

Tight-binding quantum chemical molecular dynamics method: a novel approach to the understanding and design of new materials and catalysts

Parasuraman Selvam^a, Hideyuki Tsuboi^b, Michihisa Koyama^c,
Momoji Kubo^{c,d}, Akira Miyamoto^{b,c,*}

^a Department of Chemistry, Indian Institute of Technology-Bombay, Powai, Mumbai 400 076, India

^b New Industry Creation Hatchery Center, Tohoku University, 6-6-10 Aoba, Aramaki, Aoba-ku, Sendai 980-8579, Japan

^c Department of Applied Chemistry, Graduate School of Engineering, Tohoku University, 6-6-07 Aoba, Aramaki, Aoba-ku, Sendai 980-8579, Japan

^d PRESTO, Japan Science and Technology Agency, 4-1-8 Honcho, Kawaguchi, Saitama 332-0012, Japan

Available online 29 January 2005

Abstract

Computational chemistry has made tremendous impact on the development of a variety of new materials including catalysts, semiconductors, ceramics, polymers, functional materials, etc. Traditionally, first-principles calculations were employed to clarify the chemical reactions on electronic and atomic level, which is essential for the materials and catalysts design. However, this method cannot simulate the chemical reaction dynamics at reaction temperatures, which is crucial fault and defect for more precise and accurate design to establish next-generation nanotechnology. Recently, first-principles quantum chemical molecular dynamics (QCMD) approach is expected to solve the above problem, however it can simulate very small system because it requests huge computational costs. Hence, recently we have succeeded in developing a tight-binding quantum chemical molecular dynamics (TB-QCMD) program, “Colors”, based on our original tight-binding theory. This method realizes over 5000 times acceleration in calculation time, compared to the conventional first-principles molecular dynamics method. To realize high accuracy in spite of the above high calculation speed, all the parameters for “Colors” were determined on the basis of first-principles density functional calculations. Thus, this novel TB-QCMD program was used successfully and effectively to investigate chemical reaction dynamics of large simulation models at reaction temperatures. In this review, we put forward the application of this newly developed code for the design of novel materials and catalysts systems.

© 2005 Elsevier B.V. All rights reserved.

Keywords: Tight-binding quantum chemical molecular dynamics; Chemical reaction dynamics; Large-scale calculations; Materials; Catalysts

1. Introduction

In recent years, computational chemistry has made spectacular progress and tremendous impact on the development of a variety of engineering materials. It has also been extensively used to identify, optimize, and rationally select new materials. Studies at atomic and electronic level are expected to play a key role in predicting new materials with unusual characteristics. Since experimental information at atomic scale is scarce, computational chemistry approach is

particularly desirable. Previously, computational chemistry was mainly used to elucidate the physico-chemical properties, however recently it contributes much to the design of new materials and catalysts as well as to predict the unexplored properties by the significant advancement of the theory and simulation algorithms.

Among numerous computational methods, first-principles quantum chemical approach is most powerful. However, previously first-principles quantum chemical calculations required the use of models consisting of a finite number of atoms (a cluster). This approach was the earliest to be used due to its low computational cost. However, this method suffers from several disadvantages, and has adverse effect on the computed results as the cluster model approach largely

* Corresponding author.

E-mail addresses: selvam@iitb.ac.in (P. Selvam),
miyamoto@aki.che.tohoku.ac.jp (A. Miyamoto).

depends on the cluster size [1–3]. Hybrid quantum mechanics/molecular mechanics approach overcomes the problem of neglecting the long-range electrostatic interactions, where the active site is treated by quantum mechanics while the rest is treated by molecular mechanics. This approach presents a new method for calculating large number of atoms with small and specific active site (in catalysts. For example, this methodology was applied to) the acidity in zeolites with different structural topologies [4]. However, the accuracy of this method is still under debate. Recent advances of the first-principles quantum chemical calculations realized the investigation on the two-dimensional or three-dimensional periodic systems of the materials and catalysts. This approach is expected to solve the problem of the cluster model calculations, however still small amount of the atoms in unit cell can be considered because of its huge computational costs. The periodic structure with small number of atoms does not reflect the realistic materials and catalysts and hence in this moment this periodic approach cannot apply to the complicated problems.

On the other hand, electronic structure calculations, such as first-principles quantum chemical calculations, are usually performed for a static atomic structure, while the dynamical behaviors, e.g., proton transfer or dynamic behavior of guest molecules interacting with acidic sites in zeolites can be investigated by performing classical molecular dynamics (MD) or kinetic Monte Carlo (MC) simulations. However, these approaches employ empirical interatomic potentials and hence they cannot be applied to the unknown system and cannot predict new phenomena. Moreover, the chemical reaction dynamics at reaction temperatures cannot be simulated by these approaches, because electron is not directly considered in these calculations. These are crucial faults of the classical simulation approaches for the design of new materials and catalysts.

Hence, more recently, a first-principles quantum chemical molecular dynamics (QCMD) method is expected to overcome the above problems of the static quantum chemical methods and classical simulation approaches. Especially, it enables us to clarify the chemical reaction dynamics at reaction temperature, which is essential for the materials and catalysts design in the next-generation nanotechnology. However, the first-principles QCMD demands extremely huge computational costs and hence it can simulate only small models. In order to establish a novel methodology for real systems, recently, we have successfully developed a tight-binding quantum chemical molecular dynamics (TB-QCMD) code “Colors” based on our original tight-binding theory [5–10]. This new code realizes over 5000 times acceleration in the calculation time, compared to the conventional first-principles QCMD programs. Hence, this new method can simulate the chemical reaction dynamics at reaction temperatures with much larger models and allows for the prediction of important properties of large molecules and solid systems. Especially, this method

realized the investigations on hetero-interfaces, small amount of dopants, defects, solvents, nano-structures, and other complex systems. At this juncture, it is important to mention here that our TB-QCMD predictions for large-sized molecules/solids systems have the same accuracy as that achieved from first-principles calculations and high quality experimental data, since all the parameters employed in this TB-QCMD method are determined on the basis of the first-principles calculation results. Thus, our new TB-QCMD code has been effectively employed to investigate various chemical systems and to clarify the chemical reaction and electron transfer dynamics at reaction temperatures [11–15]. In this review, the applications and the perspective of our new method will be highlighted.

2. Tight-binding quantum chemical molecular dynamics method

In our TB-QCMD method total energy, E , is given by the following expression:

$$E = \sum_{i=1}^n \frac{m_i v_i^2}{2} + \sum_{k=1}^{\text{occ}} \varepsilon_k + \sum_i \sum_{j>i} \frac{Z_i Z_j e^2}{R_{ij}} + \sum_i \sum_{j>i} E_{\text{rep}}(R_{ij}) \quad (1)$$

where the first, second, third, and fourth terms represent the kinetic energy of the nucleus, the summation of the eigenvalues of all occupied orbitals, the Columbic interaction energy, and the exchange-repulsion interaction energy, respectively. Here, m and v are mass and velocity of atoms respectively, Z_i and Z_j are the charges of atoms, e is the elementary electric charge, and R_{ij} is the internuclear distance. The exchange-repulsion term, $E_{\text{rep}}(R_{ij})$ is given by:

$$E_{\text{rep}}(R_{ij}) = b_{ij} \exp\left(\frac{a_{ij} - R_{ij}}{b_{ij}}\right) \quad (2)$$

where a_{ij} and b_{ij} are parameters related to the size and stiffness of the atoms, respectively. From the derivative of Eq. (1), we obtain the atomic force:

$$F_i = \sum_{j \neq i} \sum_{k=1}^{\text{occ}} C_k^T \frac{\partial H}{\partial R_{ij}} C_k + \sum_{j \neq i} \sum_{k=1}^{\text{occ}} \varepsilon_k C_k^T \frac{\partial S}{\partial R_{ij}} C_k - \sum_{j \neq i} \frac{Z_i Z_j e^2}{R_{ij}^2} + \sum_{j \neq i} \frac{\partial E_{\text{rep}}(R_{ij})}{\partial R_{ij}} \quad (3)$$

where H is the Hamiltonian matrix, S is the overlap integral matrix, C is the eigenvector matrix, C^T is the transposed matrix of the eigenvector matrix, and ε_k is the orbital energy. Higher accuracy was achieved by our new parameterization procedure based on the first-principles density functional theory (DFT) calculations. To determine the parameters for the “Colors” program, DFT calculations were carried out with the Amsterdam Density Functional (ADF) program [16]. The ADF [16] and DMol³ [17] programs were employed to validate the accuracy of our TB-QCMD method

by the comparison of the calculation results. The simulation results of TB-QCMD were visualized by the New-RYUGA program developed in our laboratory [18].

3. Chemical reaction dynamics over organometallic catalysts [19–22]

The strained methylenecycloalkanes, e.g., methylenecyclopropane (MCP) and methylenecyclobutane (MCB), often undergo ring opening reactions promoted by single-site metallocene-based complexes, which has been effectively utilized in organic synthesis, polymerization/copolymerization or cycloaddition with alkenes [19]. An interesting but often problematic feature of MCPs is their multiform reactivities that may lead to the formation of a variety of products by the opening of proximal and distal bonds as well as C=C double bond addition reaction. Furthermore, with the appropriate choice of metals and ligands, the ring-opening polymerization proceeds either by 1,2-insertion or by 2,1-insertion (Fig. 1). Moreover, the reactivity of MCP also varies significantly with the size of the lanthanide ion. Despite the widespread investigation, a full understanding of the reaction mechanism is still far from complete. In addition, much less attention has been paid to the roles of organolanthanide, (Cp_2LnH ($\text{Cp} = \eta^5\text{-C}_5\text{H}_5$, $\text{Ln} = \text{La}$ or Lu) that promote MCP ring-opening process. Therefore, the study of MCP ring-opening in relation to its reactivity and

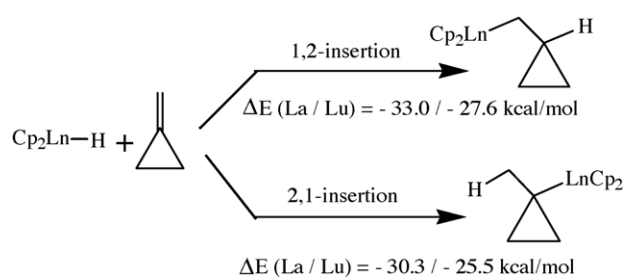


Fig. 1. Insertion types of Cp_2LnH -MCP ($\text{Ln} = \text{La}$ or Lu) systems [19].

reaction mechanism is of fundamental importance. Theoretical studies are still relatively few owing to the fact that such studies require huge computational time and moreover, the systems are highly complicated due to the large relativistic effects [23–27]. Although with modern first-principles DFT methods, total energies of useful accuracy are readily available for given molecular structures of real size systems, transition state search is still very time consuming, and constitutes a bottleneck in the study of real systems [19–22]. While the use of modest bases and simplified treatment of electron correlation extend the range of systems that may be studied with a reasonable effort [23–27], the first-principles methods still leave many chemically interesting ligands and substituents out of reach.

On the other hand, our TB-QCMD method is much faster and it has high accuracy comparable to first-principles QCMD calculation. Moreover, this novel powerful program was successfully used to investigate several chemical reactions and chemical reaction dynamics of large simulation model systems, and it well reproduced the real electronic structure and bonding of the material obtained from the first-principles results [28–30]. Hence, we performed TB-QCMD calculation of the ring-opening of MCP assisted by Cp_2LaH using “Colors” code. At first, the initial structures of MCP and Cp_2LaH were geometrically optimized (Fig. 2) by “Colors” [31], and the results are in good agreement with the first-principles DFT calculations using ADF as well as with the literature data [32–35]. The dynamic simulation of the ring-opening of MCP was then performed using “Colors”. Fig. 3 depicts the variation in bond population against the simulation time for the ring-opening process of MCP over Cp_2LaH catalyst. The results indicate the formation of Cp_2LaH -MCP complex by 1,2-insertion with a subsequent hydrogen transfer followed by the ring-opening of the proximal bond (Fig. 4). Thus, it can also be presumed that the other lanthanide metallocene catalysts such as Cp_2LuH may follow a similar ring-opening pathway. However, with additional MCP, either a smooth polymerization or a dimerization (Fig. 5) may occur [36,37].

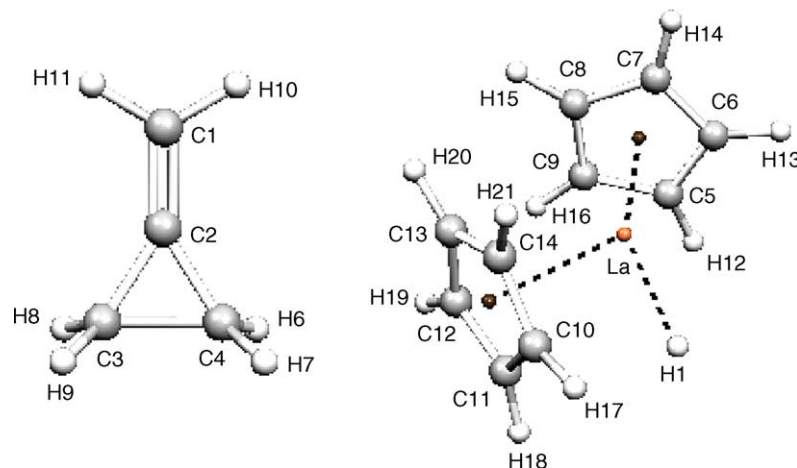


Fig. 2. Optimized models of the substrate (MCP) and the catalysts (Cp_2LnH ; $\text{Ln} = \text{La}$ or Lu) [31].

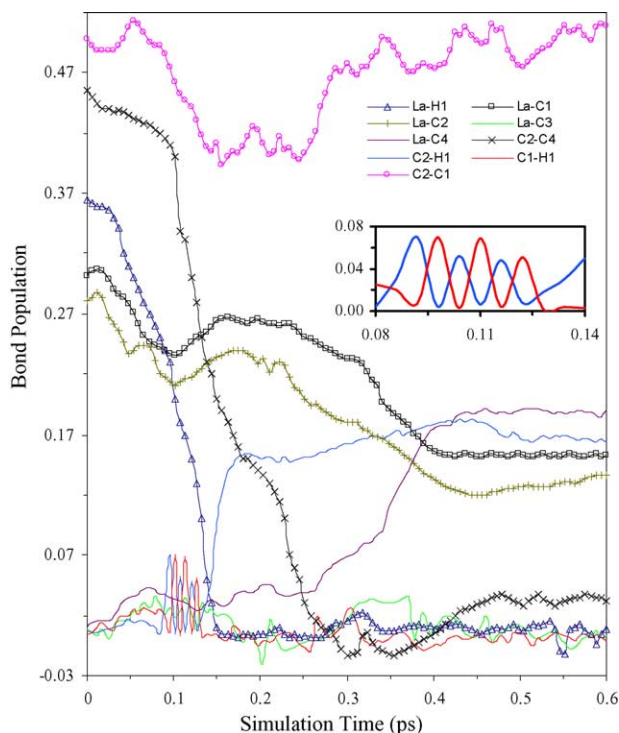


Fig. 3. Bond population during the ring-opening of MCP over Cp_2LaH with a time interval of 0.2 fs under reaction temperature (298 K). The insert presents the bond population of $\text{C}_1\text{-H}_1$ and $\text{C}_2\text{-H}_1$ bonds from 0.08 to 0.14 ps, respectively [9].

This ring-opening mechanism is well supported by the snapshots and the overlap bond population, where the formation of new C–H and La–C bonds and the dissociation of La–H and proximal C–C bonds can be tracked very well [9]. The obtained dynamic ring opening mechanism is similar to the static mechanism derived from DFT calculation [19]. Although the dynamic effect was found to alter the rearrangement mechanism of protonated pinacolyl alcohol ($\text{Me}_3\text{C-CHMe-OH}_2^+$) [38], it is not true for the ring-opening of MCP. Furthermore, A novel transition state was proposed for insertion reaction of alkenes, where tetrahedral η^4 -coordination structure was observed and hence differs from the traditional planar η^2 -coordination structure.

4. Electronic states dynamics of supported metal catalysts [39,40]

Metal supported or doped CeO_2 is widely used as environmental catalyst [41]. It was found that Cu/CeO_2 or CuO/CeO_2 catalyst system was found to be very effective for steam reforming of methanol [42], wet air oxidation of phenol [43], NO reduction [44] and the oxidation of CO [44,45] at low temperature. However, the interaction between Cu and Ce as well as their influence on the activation are not well understood. Moreover, several experimental studies showed the formation of $\text{Ce}_{1-x}\text{Cu}_x\text{O}_{2-\delta}$ solid solution with low Cu

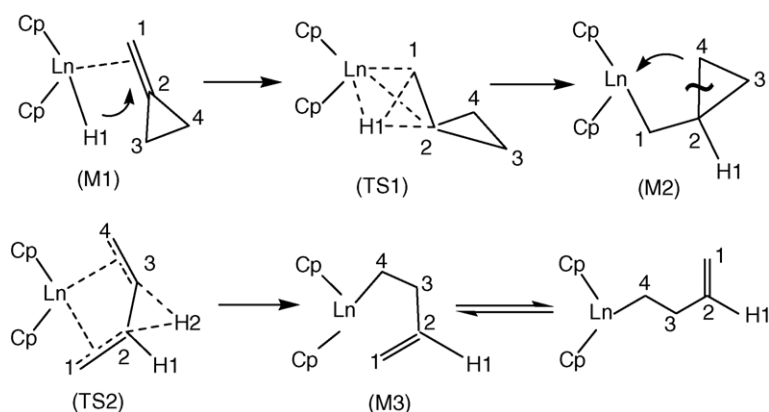


Fig. 4. Ring-opening pathway of MCP over Cp_2LnH ($\text{Ln} = \text{La}$ or Lu) catalyst [19].

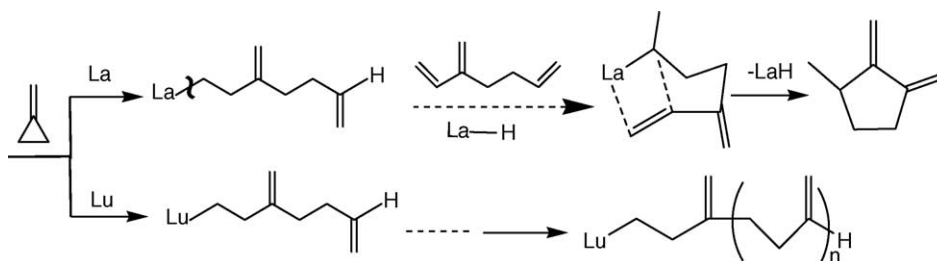


Fig. 5. Dimerization and polymerization pathways of MCP over Cp_2LnH ($\text{Ln} = \text{La}$ or Lu) [31].

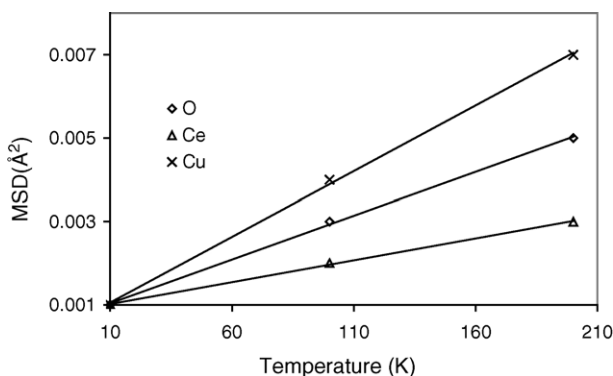


Fig. 6. Temperature dependence of mean square displacement (MSD) of Ce, Cu, and O in $\text{Ce}_{1-x}\text{Cu}_x\text{O}_{2-\delta}$ [39].

content [46]. To the best of our knowledge, no literature data is available on the theoretical study of $\text{Ce}_{1-x}\text{Cu}_x\text{O}_{2-\delta}$ catalyst system, although the motion of Ca ion in doped ceria was investigated by classical MD simulation [47].

Hence, here we present our applications of the TB-QCMD code to the atomistic dynamics of $\text{Ce}_{1-x}\text{Cu}_x\text{O}_{2-\delta}$ catalyst considering the electron transfer and electronic states dynamics. Fig. 6 shows that the mean square displacement (MSD) of Ce, Cu and O atoms in $\text{Ce}_{1-x}\text{Cu}_x\text{O}_{2-\delta}$ solid as a function of temperature obtained by our ‘‘Colors’’ code [39]. It can be seen from this figure, the calculated values vary linearly with temperature. Such a relationship is expected for a solid where anharmonic forces are not too dominating. A similar correlation was also reported for CeO_2 [48]. The MSD of Cu is larger than that of O and Ce, which indicates that it is highly difficult for the doped Cu to keep the lattice site of Ce because of the smaller ionic size. Furthermore, we also performed TB-QCMD simulation on the surface model of $\text{Ce}_{1-x}\text{Cu}_x\text{O}_{2-\delta}$ catalyst [40]. As shown in Fig. 7, the simulation result, for the first time, showed orbital overlap between Cu and Ce in $\text{Ce}_{1-x}\text{Cu}_x\text{O}_{2-\delta}$ catalyst. The associated orbital composition indicated the atomic contribution from Cu and Ce. The coupling of atomic orbital between Cu and Ce may make the

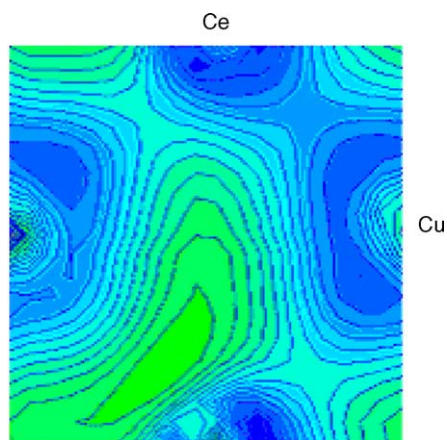


Fig. 7. Orbital isosurface from TB-QCMD simulation on periodic surface $\text{Ce}_{1-x}\text{Cu}_x\text{O}_{2-\delta}$ (110) model [40].

valence change easier between Cu^{2+} and Cu^+ and hence the catalyst keeps high activity. The results are in good agreement with the DFT calculations [49].

5. Large scale calculation on supported metal catalysts [14]

Precious metals such as Rh, Pd and Pt are essential ingredients for the three-way automotive exhaust catalyst. A uniform dispersion of the metal particles is necessary for the enhancement of the catalytic activity as well as for the reduction in the catalyst cost. Hence, various metal oxide supports have been utilized for the preparation of well-dispersed supported metal catalysts [50,51]. Among the numerous precious metal supported catalyst systems, e.g., Pt/ ZrO_2 , Pt/ TiO_2 , Pt/ Al_2O_3 , etc., the Pt/ ZrO_2 finds special attention owing the stability in wide temperature range, and the latter two are deactivated under a similar experimental conditions [52]. However, only very few theoretical studies have been performed on the zirconia supported precious metal catalysts [53].

Hence, we introduce here our successful applications of the TB-QCMD method to the complicated interface characteristics of precious metal containing cubic zirconia (c- ZrO_2) catalysts, viz., M/c- ZrO_2 (M = Rh, Pd or Pt). We selected two types of isolated Pt clusters, i.e., Pt_{13} and Pt_{55} , and one c- ZrO_2 (111) supported Pt_{13} cluster systems [14]. Fig. 8a depicts the Pt_{55} cluster model, while Fig. 8b shows the c- ZrO_2 (111) supported Pt_{13} cluster model. Table 1 shows the Pt cluster properties after geometrical relaxation by TB-QCMD and DFT methods. This result reveals that the ‘Colors’ code gives us accurate properties on Pt_{13} cluster calculation. Furthermore, the ‘Colors’ results indicate that the Pt_{55} cluster has -0.12 of surface Pt atomic charge while the Pt_{13} cluster shows -0.017 of surface Pt atomic charge, which suggests that the negative surface charge could be related to the metal particle size. The charge transfer in Pt particles has a tendency of negative surface charge, while the inner atoms of particle have positive charge (Fig. 9a). It is interesting to note that the c- ZrO_2 (111) supported Pt_{13} cluster surface shows more complicated charge distribution (Fig. 9b) than the free Pt particle (Fig. 9a), which can be

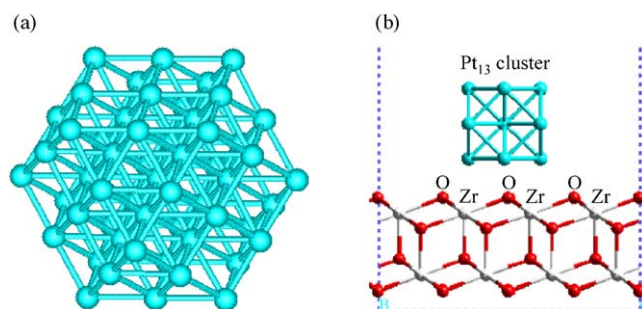


Fig. 8. (a) Isolated Pt_{55} cluster and (b) supported Pt_{13} cluster on c- ZrO_2 (111) surface [14].

Table 1
Optimized free Pt particle properties [14]

	DFT-Pt ₁₃	Colors-Pt ₁₃	Colors-Pt ₅₅
Binding energy (eV)	-53.2	-53.5	-399.2
Surface Pt charge	-0.012	-0.017	-0.120
Surface Pt–Pt length (Å)	2.623	2.620	2.626

explained by the effects of ZrO₂ support. It can also be seen from Fig. 9b that the supported Pt₁₃ particle has positive total charge; especially Pt atoms bonded with ZrO₂ surface show larger positive charge while other Pt atoms have almost neutral charge or negative charge. Thus, it was deduced from this study that the free Pt clusters have completely negative surface charge while the supported metal particle has variable surface charge. The different surface charge of the latter could be attributed to the observed unusual catalytic activity. Finally, we confirmed that our TB-QCMD code is very efficient and effective to investigate the metal–support interactions by using huge simulation models, which cannot be realized by the traditional first-principles method.

6. Chemical reaction dynamics over Ziegler–Natta catalyst [54]

Ziegler–Natta catalyst is extensively used to polymerize ethylene and propylene to their homo- and co-polymers [55]. However, the identification of active sites and control of polymerization are difficult challenges. A better understanding of catalytic systems leads to great practical advancements in the efficiency and economy of industrial polymerization processes. Large number of experimental studies has been made on this subject, and the structural and mechanistic information of active sites has been inferred from product analysis. However, the details remain unclear because these processes proceed via many surface intermediates that are not identifiable with product analysis. Moreover, only very little is known about the reaction itself because of the difficulties encountered with the experimental studies. Hence, here we introduce our successful applications of the TB-QCMD method to the polymerization

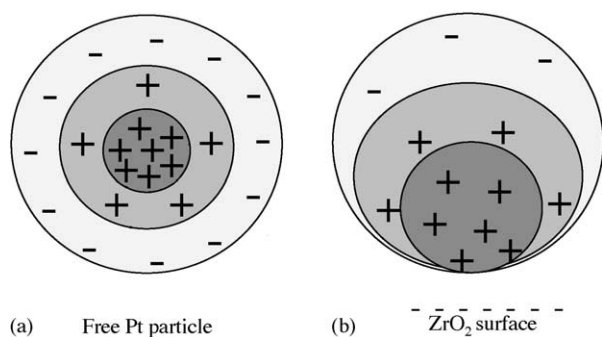


Fig. 9. Concept diagram for the charge distribution of (a) free Pt particle and (b) Pt₁₃ particle on c-ZrO₂ (111) surface [14].

reaction dynamics of propylene on Ti-based Ziegler–Natta catalyst at reaction temperature [54].

MgCl₂ (100) and MgCl₂ (110) surfaces are thought as the best useful supports for Ti-based Ziegler–Natta catalyst, and among our large number of simulation results we demonstrate here the catalytic reaction dynamics of propylene molecule on the Ti/MgCl₂ (110) catalyst. We constructed our model by replacing one of the exposed Cl atoms connecting to Ti with a C₂H₅ group as an activated center of MgCl₂ (110) surface. Fig. 10 shows the insertion process of the first propylene molecule to Ti fourfold activated site on the MgCl₂ (110) surface at 343 K. Our results show that a π -complex can be formed in a barrierless way and the molecule is oriented at the position as shown in Fig. 10b. There is no steric hindrances between the ethyl group in the incoming propylene and the growing polymer chains. Thus, a stable complex is generated. Our results indicated that the complexation energy is reduced in the polymerization of propylene molecule in comparison with that of ethylene, which is about 21.1 kcal/mol in propylene and 24.0 kcal/mol in ethylene. This difference is originated from the fact that the Ti-alkene distance is larger in Ti-propylene than that in Ti-ethylene, resulting in a lower complexation energy. The energy difference between the final product (Fig. 10d) and the initial structure (Fig. 10a) of this insertion reaction is 13.5 kcal/mol. The lower energy of Fig. 10d indicates a more stable structure of the growing polymer chain has been formed. This energy difference is very close to that of the first propylene insertion to fivefold activated site (12.6 kcal/mol) in the successive insertion reactions reported by other research. Furthermore, these results support the reaction mechanism of the propylene insertion process proposed by experiments.

7. Large-scale calculations on adsorption and electron transfer dynamics on metal surface [10]

The reactivity of carbon–carbon (C–C) and carbon–hydrogen (C–H) bonds over metal surfaces has become the subject of current interest as it can provide valuable information towards elucidating the initial elementary reaction mechanisms as well as understanding the modes of activation at the molecular level. Although, the molecular level surface chemistry of hydrocarbons has extensively been studied and tremendous progress has been made, a detailed description of the adsorption remains a challenge to the scientific community, especially for adsorbates. Thus, considerable attention has been focused to the activation of saturated cyclic hydrocarbons [10], with a special emphasis on cyclopropane (c-C₃H₆), which can serve as an ideal probe molecule in studies of hydrocarbon transformation reactions on different metal surfaces. Chemically, c-C₃H₆ is an attractive adsorbate for several reasons: although c-C₃H₆ is a saturated molecule, it possesses both olefinic and paraffinic character (C–C = 1.511 Å; \angle HCH = 114.3°); it has a

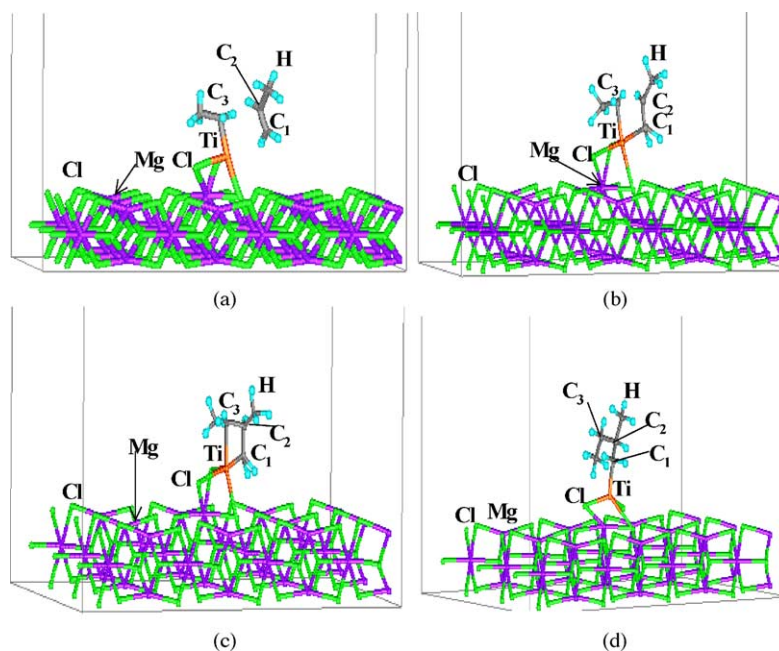


Fig. 10. Insertion process of the first propylene molecule to Ti fourfold activated site on the MgCl_2 (110) surface. (a) Initial structure, (b) π -complex, (c) transition state, and (d) final product [54].

relatively weak C–C bond energy of 289 kJ/mol as compared to 347 kJ/mol for normal hydrocarbons; further the strain energy associated with the ring is 115 kJ/mol and the C–H bond strength (419 kJ/mol) exceeds that in normal alkanes (404 kJ/mol). The relative high reactivity of $c\text{-C}_3\text{H}_6$, as a consequence of highly strained C–C bonds, results in its use as a simple probe molecule as compared to the straight chain alkanes.

It has been found that on the copper surfaces, $c\text{-C}_3\text{H}_6$ typically adsorbs and desorbs molecularly at low temperatures with a desorption energy of about 9 kcal/mol. Under the irradiation energy of about 10 eV, the chemical adsorption intermediates can be produced by effectively breaking C–H and C–C bonds, as confirmed by the studies of the reaction of $c\text{-C}_3\text{H}_6$ on the copper surfaces [56,57]. The possible dissociative adsorption species are listed in Fig. 11. It is clear that when $c\text{-C}_3\text{H}_6$ adsorbed on the copper surfaces, the physical and chemical adsorptions occur separately at different initial conditions. The activation mechanism of C–C bond in $c\text{-C}_3\text{H}_6$ has been investigated by studying the reactivity of organometallic clusters or characterizing the reactivity of catalytic materials, in which the fundamental quantum chemical calculation and molecular dynamics simulation are proved to be suitable for modeling the surface chemistry of hydrocarbons and the unusual reactivity of $c\text{-C}_3\text{H}_6$ [58,59]. Quantum chemical calculations have been performed on the relationships between the reactivity and bonding properties of $c\text{-C}_3\text{H}_6$ for Rh and Ir complexes [60]. A Hartree–Fock ab initio method has been applied to study the $c\text{-C}_3\text{H}_6$ for the copper surface using the cluster model where the molecular ring plane of adsorbate molecule is placed parallel to the surface [61]. However, some challenging problems

develop when we model the adsorption process and identify the adsorption species for $c\text{-C}_3\text{H}_6$ on the copper surfaces. The adsorption takes place in an associative way and there is no dissociated surface species formed during the physisorption process, whereas the dissociated species appear under the irradiation at a power of about 10 eV. The molecular level descriptions including the electronic interaction and dynamic behaviors of the associative and dissociative adsorption are still not satisfactory to the scientific community. Thus, we focus our attention on the theoretical investigation of different

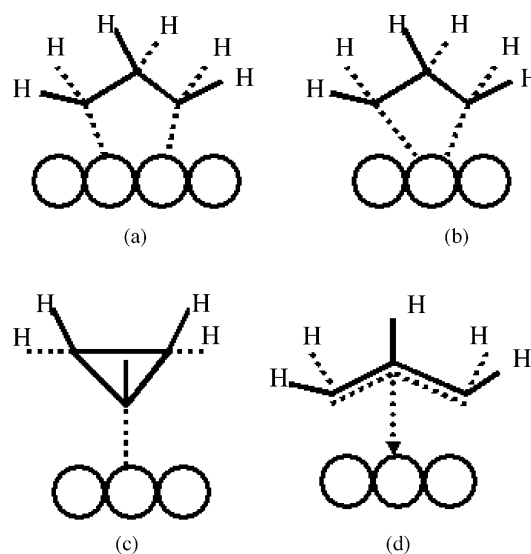


Fig. 11. Various possible adsorbed $c\text{-C}_3\text{H}_6$ species on the metal surface: (a) metallacyclopentane, (b) metallacyclobutane, (c) cyclopropyl (η^1 -allyl), and (d) cyclopropyl (π - or η^3 -allyl) [10].

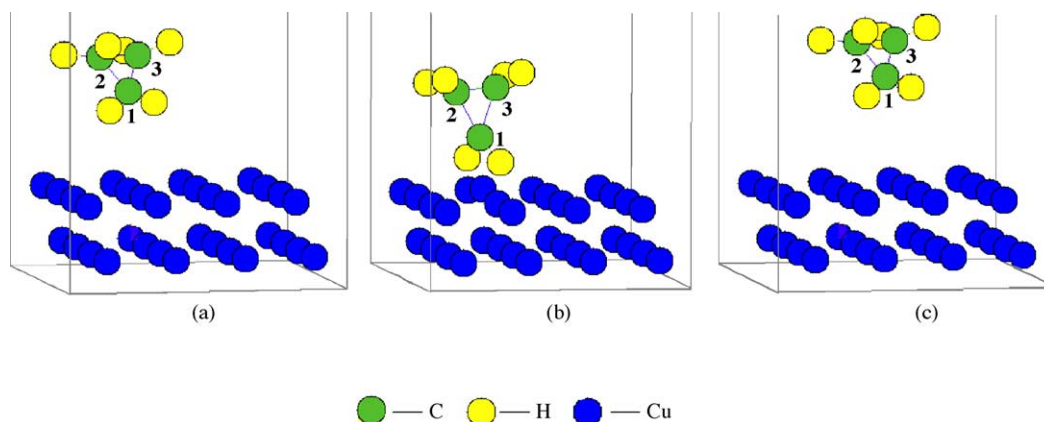


Fig. 12. Dynamics of the adsorbed $c\text{-C}_3\text{H}_6$ on copper surface at (a) 0 fs, (b) 1200 fs, and (c) 4000 fs [10].

adsorption processes with the aim of getting a deeper understanding of the activation mechanism for $c\text{-C}_3\text{H}_6$ that is adsorbed on the metal surfaces.

The dynamic behavior of this adsorption is simulated using “Colors” program. Fig. 12 presents the dynamic behavior of the $c\text{-C}_3\text{H}_6$ molecule on the copper surface. It can be seen from this figure that at the initial stages the adsorbate molecule moved towards the surface but as the time increases it moved away from the surface. The profile also shows that the distance between carbon and copper (nearest to the adsorbate) is continuously changing with the time (Fig. 13). It is also obvious from this figure that the distance between carbon and carbon nearly does not change with the time, however the distance of carbon and copper become shorter at the beginning then after reaching the minimum distance at time equals to 1200 fs, then it becomes large with a further increase of time suggesting that the desorption may also occur associatively. When the adsorbate is nearest to the copper surface, there is -0.045 electrons transferred from copper to $c\text{-C}_3\text{H}_6$ showing a weak interaction between copper surface and adsorbent molecule. The structural and electronic properties at adsorption

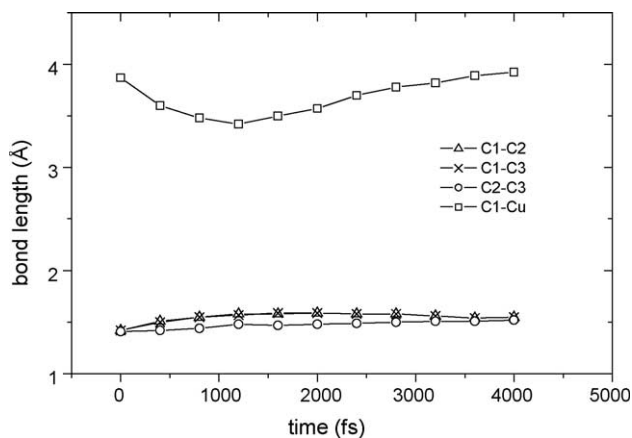
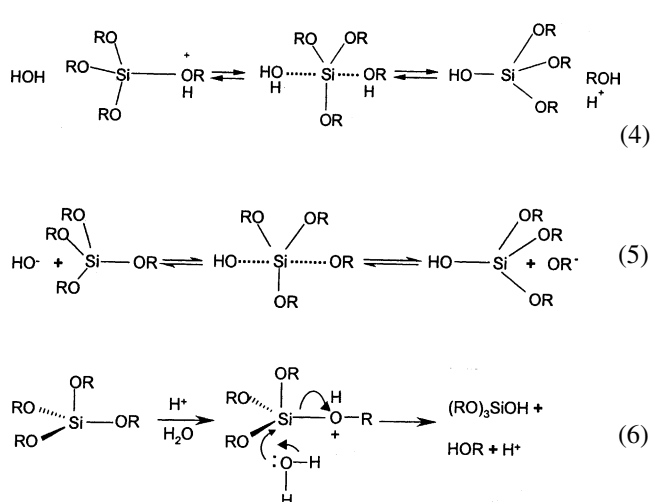


Fig. 13. Evolution of the bond distance during the adsorption process for $c\text{-C}_3\text{H}_6$ molecule on Cu surface [10].

equilibrium were also calculated by the first-principles density functional theory with periodic and cluster models using the CASTEP, Dmol³ and ADF programs. The calculated vibrational frequencies and adsorption energies are in good agreement with the experimental data. Consistently, the results indicated the tilted adsorbed geometrical structure and a weak interaction between adsorbate and adsorbent.

8. Chemical reaction dynamics of materials synthesis process [8]

The study of the hydrolyses of metal alkoxides is very important as they are fundamental reactions in the sol-gel processes, given that sol-gel processing of alkoxysilanes and organoalkoxysilanes is a promising technology for the production of certain industrially important advanced materials and coatings, e.g., glasses, ceramics, microporous (zeolites), and mesoporous molecular sieves, etc. Silicon alkoxides such as tetramethoxysilane and tetraethoxysilane are commonly employed as molecular precursors for sol-gel processing of silica [62]. In the past, several mechanisms have been put forward for the hydrolysis of the $\text{Si}(\text{OR})_4$ [8,63–65]. For both acid-catalyzed (Eq. (4)) and base-catalyzed (Eq. (5)) reactions, a $\text{S}_{\text{N}}2$ -type back-side displacement (with inversion) path was proposed. A flank-side attack mechanism (Eq. (6)) or retention (without inversion) mechanism for the acid-promoted hydrolysis process has also been suggested. However, $\text{S}_{\text{N}}2$ -type mechanism involving a stable penta-coordinate intermediate with two transition states has also been proposed under basic condition. Although the hydrolysis mechanism under neutral condition is remained unclear, a recent computational study [65] support a front-side nucleophilic attack, i.e., the alkoxide hydrolyze without inversion, which is in contrast to the back-side attack mechanism considered for the acid- and base-catalyzed hydrolysis reaction.



Our TB-QCMD method enabled us to present a clear view of the chemical reaction dynamics during the hydrolysis of $\text{Si}(\text{OCH}_3)_4$ under neutral conditions. Fig. 14 shows snapshots of the simulation of the hydrolysis reaction of $\text{Si}(\text{OCH}_3)_4$. Here, the oxygen atoms of $\text{Si}(\text{OCH}_3)_4$ are designated as O_{19} , O_{18} , O_{15} , and O_m . Likewise, the oxygen of H_2O is defined as O_w . Initially, the water molecule was placed at a distance of 1.64 Å from silicon of $\text{Si}(\text{OCH}_3)_4$. It

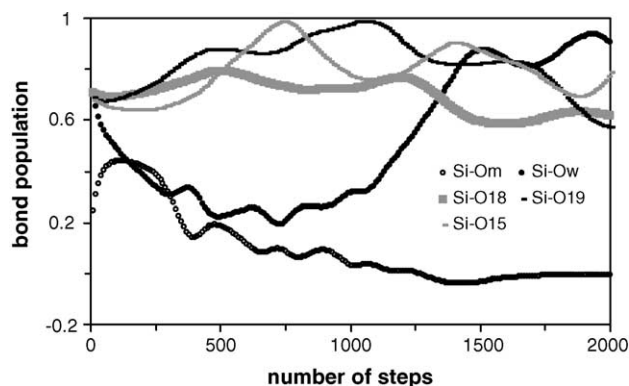


Fig. 15. Bond population of silicon and its surrounding oxygen during the hydrolysis of $\text{Si}(\text{OCH}_3)_4$ under neutral condition [8].

is clear from this figure that a flank-side attack of oxygen in water on silicon of $\text{Si}(\text{OCH}_3)_4$ (without inversion of the silicon tetrahedron) is favorable. Further, this attack makes the leaving alkoxide group diffuse away as methanol after protonation. The calculated activation energy for the hydrolysis is 22.7 kcal/mol which is comparable with the reported value of 21.6 kcal/mol. Fig. 15 depicts the bond population analysis of the interaction of $\text{Si}(\text{OCH}_3)_4$ and water during the simulation. It can be seen from this figure

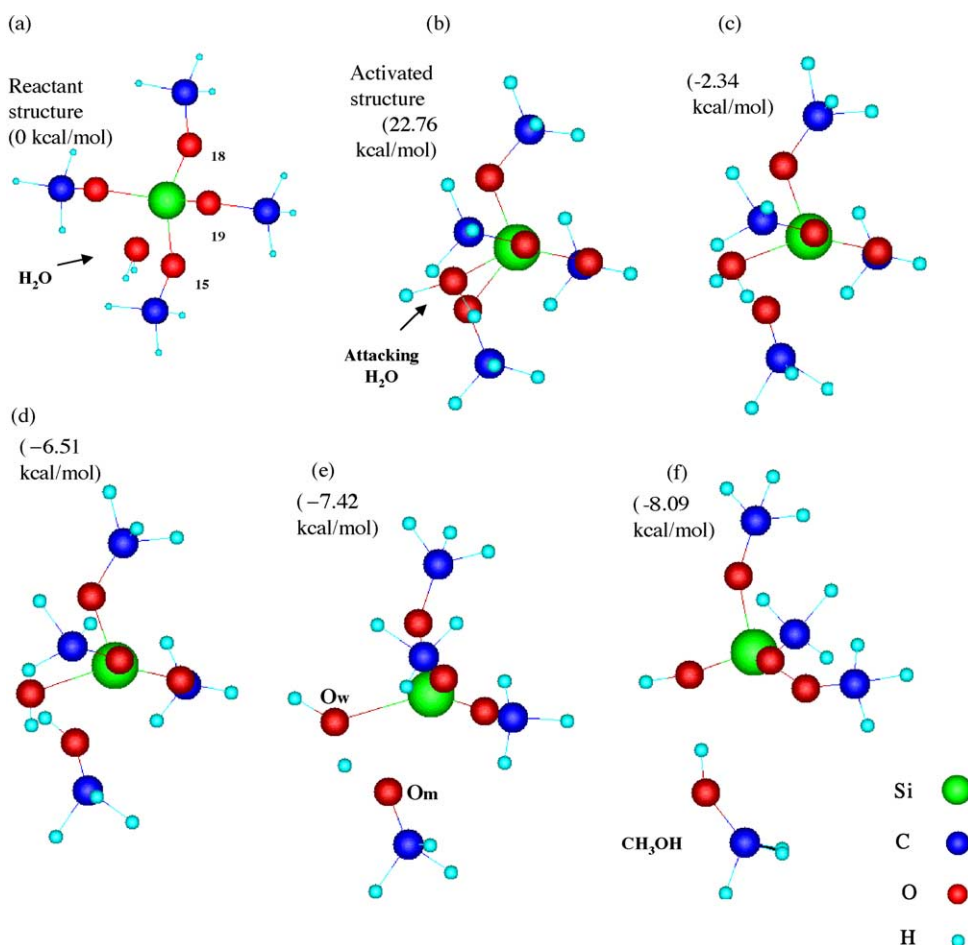


Fig. 14. Snapshots during the hydrolysis reaction of $\text{Si}(\text{OCH}_3)_4$ under neutral condition at various steps: (a) 0, (b) 50, (c) 280, (d) 400, (e) 910, and (f) 1680 [8].

that the fortification of the Si–O_w bond at the end of the simulation (or after ~1300 steps) ensuring the completeness of the hydrolysis. It can also be noted from this figure that the Si–O_w bond population is relatively high at the beginning of the simulation since it was started from the activated structure (Fig. 14b). It is interesting to note that in the midway of the simulation, the Si–O bond population, i.e., Si–O_w, Si–O_m, Si–O₁₅, Si–O₁₈, and Si–O₁₉, reveals that the formation of silicon pentacoordinate intermediate rather than siliconium ion intermediate reported previously. These results indicate that the pentacoordinate intermediate is the easy pathway for the displacement of OCH₃ by OH on Si(OCH₃)₄. In addition, we found that the proton oscillates for a period of ~60 fs between oxygen of water and oxygen of leaving methoxy group where it finally migrates to the latter to form methanol.

Furthermore, our TB-QCMD simulations revealed that the presence of the acid or base as catalyst promotes the hydrolysis by the rapid formation of Si–OH bond. Under the realistic conditions of hydrolysis, the polarity as well as the concentration of the solvent may have an influence on the type of the hydrolysis mechanism. Finally, these results suggest that our TB-QCMD code is very useful tool not only to clarify the synthesis process of materials but also to realize the theoretical optimization of the materials synthesis condition.

9. Large-scale calculation on electrode/electrolyte interface in a battery [15]

In recent years, lithium batteries have achieved great success as high energy density batteries for wide applications. Lithium secondary batteries use lithium transition metal oxides as the positive electrode and carbon as the negative electrode, which are capable of undergoing electrochemical insertion and withdrawn of the lithium ion. Among the available electrode materials, LiCoO₂ remains one of the most attractive cathode materials. LiCoO₂ [66–69] is widely used in commercially available lithium secondary batteries at present, because it can be easily prepared and gives a higher voltage as compared to other probable cathode material candidates, such as LiNiO₂ [68,69] or LiMn₂O₄ [70–72]. Although large amount of experimental information has been accumulated for LiCoO₂, theoretical approaches may also be helpful to improve the cell performance of LiCoO₂. Classical MD studies have focused on their structural properties [73], while first-principles calculations have been carried out to estimate the average voltage, energy density, and the possibility of metal reduction to other features [74–78]. In addition to the above investigations, our TB-QCMD code “Colors” enabled us to study the electronic states of complicated Li_{0.5}CoO₂/ethylene carbonate (EC) + LiPF₆ interfaces. This tight-binding approach is efficient, and it well reproduces the real electronic structure and bonding of

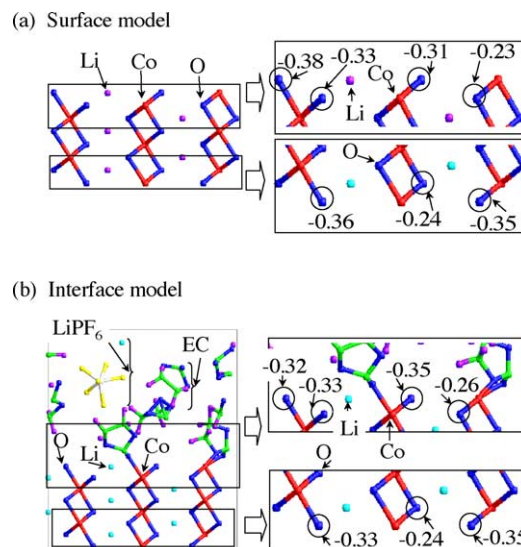


Fig. 16. Charge distributions of (a) Li_{0.5}CoO₂ (100) surface model and (b) Li_{0.5}CoO₂ electrode/EC + LiPF₆ electrolyte interface model. Atoms marked by circles represent oxygen. Right side of these figures displays the magnified view of the regions marked with the solid rectangle box [15].

materials obtained from the first-principles calculations [79,80].

We focused on the effect of the electrolyte towards the atomic charges on the surface O atoms in the Li_{0.5}CoO₂ electrode. Fig. 16a and b present the atomic charges on some specific O atoms in the Li_{0.5}CoO₂ (100) surface model and LiCoO₂ (100)/EC + LiPF₆ interface model, respectively. All the oxygen atoms in the bulk LiCoO₂ have the negative charge of –0.23. However, as shown in Fig. 16a, the oxygen atoms at the Li_{0.5}CoO₂ (100) surface have wide-range atomic charges of –0.23 to –0.38. This result suggests that some surface oxygen atoms have highly negative charge compared to those in the bulk LiCoO₂. On the other hand, it is very interesting to notice that the range of the atomic charges on the oxygen atoms in the interface model is narrower owing to the interaction of the oxygen atoms with the electrolyte, as shown in Fig. 16b. The oxygen atoms in the interface model have the atomic charges of –0.24 to –0.35. In other words, the electrolyte molecules EC + LiPF₆ stabilize the atomic charges and electronic states of the oxygen atoms at the Li_{0.5}CoO₂ (100) surface.

These results indicate that our TB-QCMD method is also effective to clarify the electronic states and electron transfer of the complicated interfaces in battery systems.

10. Chemical reaction dynamics of semiconductor manufacturing processes [12]

Plasma etching is one of the most important processes for atomic-scale fabrication of silicon semiconductor devices. A detailed understanding of the surface chemical reaction dynamics during the plasma-etching process can facilitate the development of such atomic-scale control techniques.

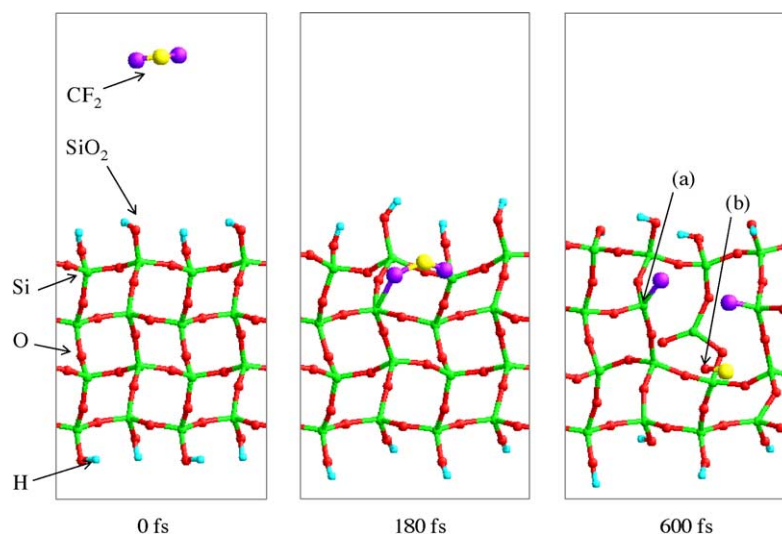


Fig. 17. Dynamic behavior of CF_2 bombardment with an incident energy of 10 eV onto SiO_2 surface. (a) and (b) show the atoms on which bond population were analyzed in Figs. 18 and 19, respectively [12].

Although a large number of experimental results related to the plasma processes have been accumulated [81–84], computer simulation methods are expected to play an important role in the advancement of the plasma technology. Among numerous available simulation methods, classical molecular dynamics approach has been used to study the surface chemical reaction dynamics in various processes [85–88]. However, this method employs empirical interatomic potential functions and does not consider the electron transfer, and hence it cannot simulate accurately the chemical reaction dynamics. In this context, our TB-QCMD code “Colors” enables us to simulate precisely the chemical reaction dynamics during the plasma etching processes on a SiO_2 surface by considering electron transfer dynamics [12]. Hence, here we introduce our successful application of the TB-QCMD code to the chemical reaction dynamics during the bombardment process of an energetic CF_2 radical onto a SiO_2 surface.

The snapshots of the TB-QCMD simulations were presented in Fig. 17, when a CF_2 radical with an incident energy of 10 eV was bombarded onto a SiO_2 substrate. This figure shows that the incident CF_2 radical intruded into the SiO_2 substrate and some complicated chemical reactions took place. In order to clarify the bond-breaking and bond-formation processes during the chemical reactions, atomic bond populations were analyzed. Fig. 18 represents the bond population on one Si atom in the SiO_2 substrate. One of the Si–O bond population immediately decreased at 200 fs, and at the same time the Si–F bond population increased. This result indicates that the bombardment of the CF_2 radical led to the Si–O bond breaking and Si–F bond formation. Fig. 19 depicts the bond population on one O atom in the SiO_2 substrate. The Si–O bond population immediately decreased at 200 fs and at the same time the C–O bond population increased. These results indicate that the bombardment of

the CF_2 radical led to the Si–O bond-breaking and the formation of CO molecule. At this juncture, it is important to note that the formation of the volatile molecules such as SiF_4 and CO was observed experimentally during the SiO_2 etching processes by the fluorocarbon plasma [89]. These results confirm that our TB-QCMD is also effective tool to realize the atomistic process design in the semiconductor manufacturing technology.

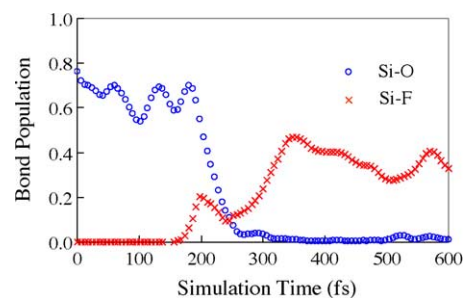


Fig. 18. Time evolution of bond population on one Si atom when a CF_2 radical with an incident energy of 10 eV was bombarded onto a SiO_2 substrate [12].

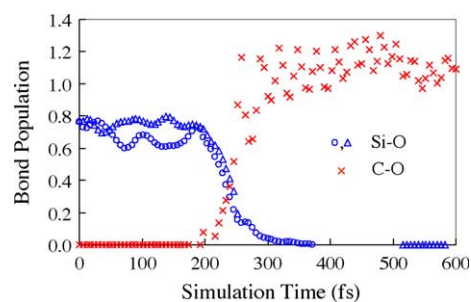


Fig. 19. Time evolution of bond population on one O atom when a CF_2 radical with an incident energy of 10 eV was bombarded onto a SiO_2 substrate [12].

11. Degradation reaction dynamics of lubricants in mechanical engineering [13]

Esters have important uses in the synthesis of some petroleum additives and synthetic lubricants. Among the numerous lubricants, synthetic esters are extensively used in various fields such as engine oil, refrigeration oil, hydraulic oil and cream, and so on owing to their outstanding friction properties. Furthermore, as compared to petrolatum oil, the synthetic esters have several notable properties such as biodegradation, flame resistance, lubricating ability, flowability at cold temperature, etc. In addition, they also possess remarkable characteristics such as lower volatility, thermolization and oxidation [90–92]. Long lifetime property is an important aspect for developing lubricant, and the stability of thermolization and oxidation have closed tie with it. However, thermolization and oxidation reaction occur at the same time when lubricant are used in reality. It is difficult to confirm intermediate degradation product, final degradation product and interaction among molecules.

Although other theoretical methods cannot afford to tackle the above problems, our TB-QCMD method enabled us to clarify the degradation reaction dynamics of monoester at reaction temperatures [13]. First, the degradation dynamics of acetic ester molecule at high temperatures was investigated. Simulation results show that the β -hydrogen, which locates at ethanol group, was cleaved quickly. Compared to it, α -hydrogen was cleaved slower than β -hydrogen. Each atom expressed cleavage and association with repetition, as a whole, degradation phenomenon was observed in this simulation. Since this observation agrees with experimental data, we performed TB-QCMD calculations for the chemical reaction dynamics of monoester with oxygen molecule. It is known from the experimental data [93] that the substituted esters exhibit outstanding thermolization and oxidation. In our simulation, at the initial stages, the oxygen molecule, which is placed close to the ester molecule, is cleaved. The resulting highly active oxygen atom interacts with the ethyl

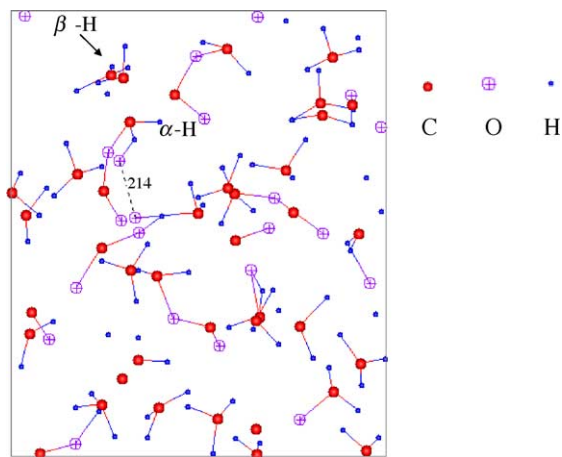


Fig. 20. Decomposition behavior of monoester under oxygen at 100 step [13].

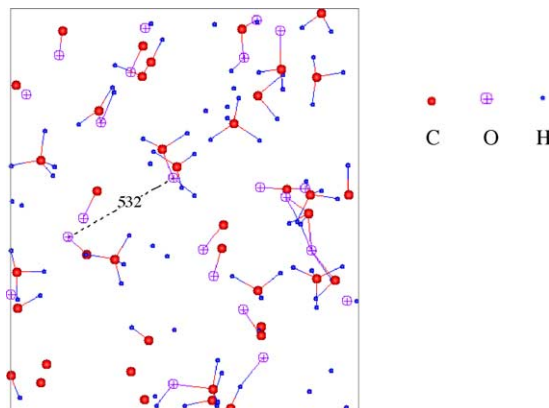


Fig. 21. Decomposition behavior of monoester under oxygen at 1300 step [13].

acetate molecule and hence the degradation of the latter takes place. However, it is noted here that the ethyl group is cleaved much more rapidly than the methyl group. In comparison, the α -hydrogen, i.e., hydrogen of the methyl group, is cleaved slower (Fig. 20) which is in good agreement with the experimental data. Thus, it can be considered that when the β -hydrogen cleaved, i.e., hydrogen of the ethyl group, the α -hydrogen begins to be unstable. As a consequence, the carbon and oxygen atoms are also unstable, and begin to contact with the closest atoms. In this way of cleavage and association with repetition, as a whole, a continuous degradation is observed during the simulation (Fig. 21). Finally, these results indicate that our TB-QCMD is useful tool not only for chemistry and physics fields but also for mechanical engineering fields.

12. Chemical decomposition dynamics of toxic and harmful compounds [11]

Polychlorinated biphenyls (PCBs) and polychlorinated dibenzodioxins (PCDDs) are known as persistent organic pollutants, which are extremely toxic and highly harmful chemical compounds. They are emitted into the environment mostly from incomplete combustion or incineration of organic wastes containing halogens [94]. The difficulties of dioxin destruction arise from not only its high chemical stability but also the formation of more toxic dioxins in incinerators. In order to develop more efficient technology to reduce the above pollutants, the detailed understanding of the decomposition mechanism of the PCBs and PCDDs has been required. However, the experiments for the decomposition of the above pollutants are quite dangerous because of their toxicity. Consequently, theoretical methods are expected to play a key role and so far only few theoretical studies on the chemical reaction pathways for these molecules have been reported [95–97]. Hence, here we introduce the effectiveness of our TB-QCMD code to clarify the chemical reaction mechanism of the decomposition processes of the PCBs and PCDDs.

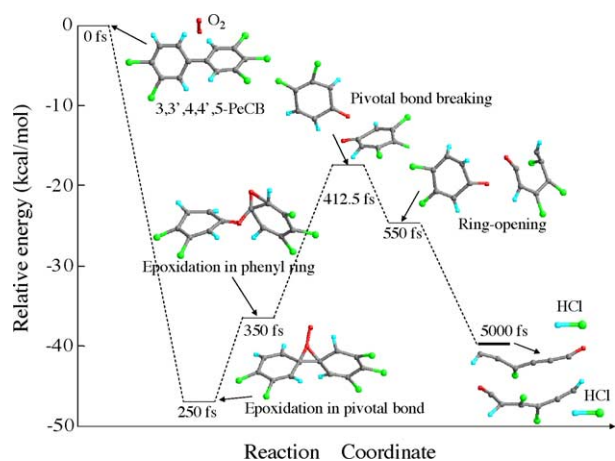


Fig. 22. Oxidative decomposition reaction dynamics of 3,3',4,4',5-PeCB at 473.15 K calculated by Colors. Relative energy to $O_2 + 3,3',4,4',5$ -PeCB is shown [11].

It is well known that 3,3',4,4',5-penta-chlorinated biphenyl (3,3',4,4',5-PeCB) and 2,3,7,8-tetrachlorinated dibenzo-*p*-dioxin (2,3,7,8-TCDD) are the most toxic compounds among the PCBs and PCDDs, respectively. Hence, we applied our TB-QCMD code “Colors” to the investigations on the oxidative decomposition reaction dynamics of the 3,3',4,4',5-PeCB, 2,3,4,4',5-PeCB, and 2,3,7,8-TCDD by O_2 molecule at 473.15 K [11]. Fig. 22 shows the oxidative decomposition process of the 3,3',4,4',5-PeCB. Initially an epoxide is formed on the pivotal bond at 250 fs and followed by the epoxidation in the phenyl ring at 350 fs. The latter is then transformed to phenoxy-like intermediate at 412.5 fs by the pivotal bond breaking. The previous theoretical calculations and experimental results proposed that the phenoxy-like intermediate leads the formation of predioxin, which is consistent with our TB-QCMD calculations. Finally, ring-opening reaction of phenoxy-like intermediate takes place between the C_1 and C_6 atoms at 550 fs. Fig. 23 shows the oxidative decom-

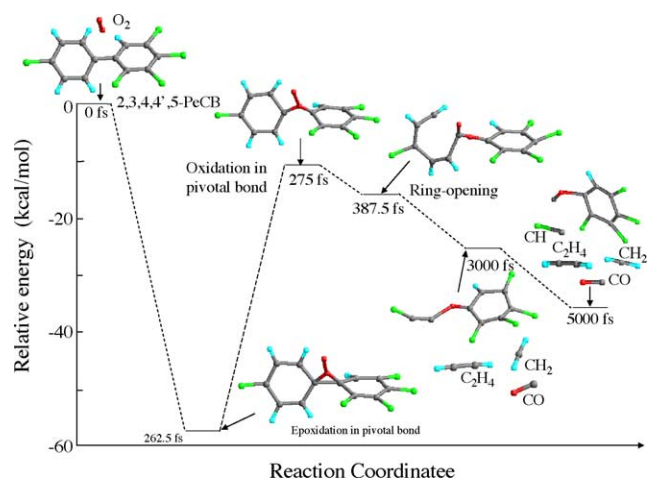


Fig. 23. Oxidative decomposition reaction dynamics of 2,3,4,4',5-PeCB at 473.15 K calculated by Colors. Relative energy to $O_2 + 2,3,4,4',5$ -PeCB is shown [11].

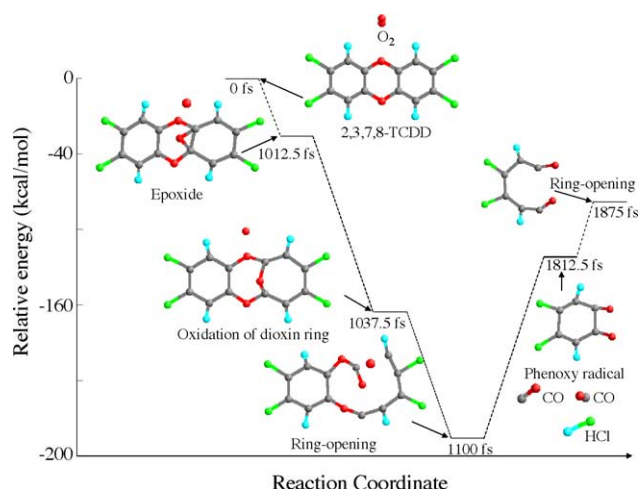


Fig. 24. Oxidative decomposition reaction dynamics of 2,3,7,8-TCDD at 473.15 K calculated by Colors. Relative energy to $O_2 + 2,3,7,8$ -TCDD is shown [11].

position process of the 2,3,4,4',5-PeCB. An epoxide is formed similarly to the decomposition process of the 3,3',4,4',5-PeCB. The initial stage at around 262.5 fs proceeds via the epoxidation and the formation of a pivotal bond, which is followed by the formation of the direct connection of two phenyl ring via oxygen, viz., oxidation in pivotal bond at 275 fs. It is noteworthy that the pivotal bond breaking of the 2,3,4,4',5-PeCB is difficult, which is quite different from the results of the 3,3',4,4',5-PeCB. Fig. 24 shows the oxidative decomposition reaction dynamics of the 2,3,7,8-TCDD. An epoxide intermediate is formed by the chemical reaction of the 2,3,7,8-TCDD and O_2 molecule at 1012.5 fs, followed by the oxidation of the dioxin ring at 1037.5 fs. Subsequently, the ring opening takes place at 1100 fs, which is then followed by the partial decomposition of the dioxin–oxygen complex to form phenoxy-like intermediate as well as other molecular fragments such as carbon monoxide and hydrogen chloride at 1812.5 fs. Finally, the phenoxy-like intermediate takes the second ring-opening reaction at 1875 fs.

These results indicate that our TB-QCMD is effective tool not only to clarify the chemical decomposition dynamics of toxic and harmful compounds but also to design the efficient technology for the decomposition of persistent organic pollutants.

13. Conclusion

The results presented in this paper suggest that our original TB-QCMD program “Colors” is very effective for the simulation of a number of physical and chemical systems. Especially, this code has been successfully applied to the clarification of the chemical reaction dynamics at reaction temperatures, which cannot be investigated by the static first-principles calculation and classical MD simulation method. The present investiga-

tion also demonstrates that the novel TB-QCMD method allows us to investigate not only simple molecules but also to extend the studies to complicated problems of industrial importance. Especially this TB-QCMD code is over 5000 times faster than the conventional first-principles QCMD approach, and then larger simulation models with several hundred of atoms can be calculated, which cannot be realized by the first-principles QCMD method. Finally we conclude that our new TB-QCMD method is very powerful tool to not only clarify the chemical reaction mechanism but also to design new materials and catalysts as well as will contribute to the solution of the complicated problems in the industry and to realize the industrial innovation.

References

- [1] E. Teunissen, R.A. van Santen, A.P. Jansen, F.B. van Duijneveldt, J. Phys. Chem. 97 (1993) 203.
- [2] J. Sauer, P. Uglieno, E. Garrone, V.R. Saunders, Chem. Rev. 94 (1994) 2095.
- [3] S.P. Yuan, J.G. Wang, Y.W. Li, H. Jiao, J. Mol. Struct. (Theochem.) 674 (2004) 269.
- [4] M. Brändle, J. Sauer, J. Am. Chem. Soc. 120 (1998) 1556.
- [5] H. Takaba, A. Endou, A. Yamada, M. Kubo, K. Teraishi, K.G. Nakamura, K. Ishioka, M. Kitajima, A. Miyamoto, A. Imamura, Jpn. J. Appl. Phys. 39 (2000) 2435.
- [6] Y. Inaba, T. Onozu, S. Takami, M. Kubo, A. Miyamoto, A. Imamura, Jpn. J. Appl. Phys. 40 (2001) 2991.
- [7] T. Yokosuka, H. Kurokawa, S. Takami, M. Kubo, A. Miyamoto, A. Imamura, Jpn. J. Appl. Phys. 41 (2002) 2410.
- [8] M. Elanany, P. Selvam, T. Yokosuka, S. Takami, M. Kubo, A. Imamura, A. Miyamoto, J. Phys. Chem. B 107 (2003) 1518.
- [9] Y. Luo, P. Selvam, Y. Ito, S. Takami, M. Kubo, A. Imamura, A. Miyamoto, Organometallics 22 (2003) 2184.
- [10] X. Wang, P. Selvam, C. Lv, M. Kubo, A. Miyamoto, J. Mol. Catal. A (Chem.) 220 (2004) 189.
- [11] A. Suzuki, P. Selvam, T. Kusagaya, S. Takami, M. Kubo, A. Imamura, A. Miyamoto, Int. J. Quantum Chem., in press.
- [12] K. Sasata, T. Yokosuka, H. Kurokawa, S. Takami, M. Kubo, A. Imamura, T. Shinmura, M. Kanoh, P. Selvam, A. Miyamoto, Jpn. J. Appl. Phys. 42 (2003) 1859.
- [13] H. Zhou, P. Selvam, K. Hirao, A. Suzuki, D. Kamei, S. Takami, M. Kubo, A. Imamura, A. Miyamoto, Tribol. Lett. 15 (2003) 155.
- [14] C. Jung, Y. Ito, A. Endou, M. Kubo, A. Imamura, P. Selvam, A. Miyamoto, Catal. Today 87 (2003) 43.
- [15] Y. Makino, T. Kusagaya, K. Suzuki, A. Endou, M. Kubo, P. Selvam, H. Ota, F. Yonekawa, N. Yamazaki, A. Miyamoto, Solid State Ionics 175 (2004) 847.
- [16] E.J. Baerends, D.E. Elis, P. Ros, Chem. Phys. 2 (1973) 41.
- [17] B. Delley, Chem. Phys. Lett. 110 (1986) 329.
- [18] R. Miura, H. Yamano, R. Yamauchi, M. Katagiri, M. Kubo, R. Vetrivel, A. Miyamoto, Catal. Today 23 (1995) 409.
- [19] Y. Luo, P. Selvam, A. Endou, M. Kubo, A. Imamura, A. Miyamoto, J. Am. Chem. Soc. 125 (2003) 2184 (and references cited therein).
- [20] Y. Luo, P. Selvam, Y. Ito, M. Kubo, A. Miyamoto, Inorg. Chem. Commun. 6 (2003) 1243.
- [21] Y. Luo, P. Selvam, M. Koyama, M. Kubo, A. Miyamoto, Inorg. Chem. Commun. 7 (2004) 566.
- [22] Y. Luo, P. Selvam, M. Koyama, M. Kubo, A. Miyamoto, Chem. Lett. 33 (2004) 780.
- [23] N. Koga, Theor. Chem. Acc. 102 (1999) 285.
- [24] L. Maron, O. Eisenstein, J. Phys. Chem. A 104 (2000) 7140.
- [25] Y. Luo, X. Wan, Y. Ito, S. Takami, M. Kubo, A. Miyamoto, Chem. Phys. 282 (2002) 197.
- [26] L. Maron, O. Eisenstein, F. Alary, R. Poteau, J. Phys. Chem. A 106 (2002) 1797.
- [27] C. Boehme, G. Wipff, Inorg. Chem. 41 (2002) 727.
- [28] J.V. Ortiz, R. Hoffmann, Inorg. Chem. 24 (1985) 2095.
- [29] M. Meuwly, M. Karplus, J. Chem. Phys. 116 (2002) 2572.
- [30] Q. Cui, M. Elstner, M. Karplus, J. Phys. Chem. B 106 (2002) 2721.
- [31] Y. Luo, Ph.D. Thesis, Tohoku University, 2003.
- [32] H.J.P. De Lijser, D.R. Arnol, J. Phys. Chem. 100 (1996) 3996.
- [33] D.R. Lide (Ed.), Handbook of Chemistry and Physics, 79th ed. CRC, Washington, 1998.
- [34] G. Lanza, I.F. Fragalà, T.J. Marks, Organometallics 20 (2001) 4006.
- [35] L. Maron, O. Eisenstein, J. Am. Chem. Soc. 123 (2001) 1036.
- [36] X. Yang, A.M. Seyam, P.-F. Fu, T.J. Marks, Macromolecules 27 (1994) 4625.
- [37] L. Jia, X. Yang, A.M. Seyam, I.D.L. Albert, P.-F. Fu, S. Yang, T.J. Marks, J. Am. Chem. Soc. 118 (1996) 7900.
- [38] S.C. Ammal, H. Yamataka, M. Aida, M. Dupuis, Science 299 (2003) 1555.
- [39] Y. Luo, Y. Ito, T. Kusagaya, A. Endou, M. Kubo, P. Selvam, A. Imamura, A. Miyamoto, Abstract of 91st Catal. Soc. Meeting, Japan, Yokohama, 26–27 March 2003, p. 40.
- [40] Y. Luo, Y. Ito, H. Zhong, A. Endou, M. Kubo, S. Manogaran, A. Imamura, A. Miyamoto, Chem. Phys. Lett. 384 (2004) 30.
- [41] J. Kašpar, M. Graziani, P. Fornasiero, in: K.A. Gschneidner, Jr., L. Eyring (Eds.), Handbook on the Physics and Chemistry of Rare Earths, vol. 29, Elsevier, New York, 2000 (Chapter 184).
- [42] Y. Liu, T. Hayakawa, T. Tsunoda, K. Suzuki, S. Hamakawa, K. Murata, R. Shiozaki, T. Ishii, M. Kumagai, Top. Catal. 22 (2003) 205.
- [43] S. Hocévar, J. Batista, J. Levec, J. Catal. 184 (1999) 39.
- [44] P. Bera, S. Mitra, S. Sampath, M.S. Hegde, Chem. Commun. (2001) 927.
- [45] A. Martínez-Arias, R. Cataluña, J.C. Conesa, J. Soria, J. Phys. Chem. B 102 (1998) 809.
- [46] P. Bera, K.R. Priolkar, P.R. Sarode, M.S. Hegde, S. Emura, R. Kumashiro, N.P. Lalla, Chem. Mater. 14 (2002) 3591.
- [47] S. De Carolis, J.L. Pascual, L.G.M. Pettersson, M. Baudin, M. Wójcik, K. Hermansson, A.E.C. Palmqvist, M. Muhammed, J. Phys. Chem. B 103 (1999) 7627.
- [48] M. Baudin, M. Wójcik, K. Hermansson, Surf. Sci. 468 (2000) 51.
- [49] S.C. Su, A.T. Bell, J. Phys. Chem. B 102 (1998) 7000.
- [50] Z. Dang, B.G. Anderson, Y. Amenomiya, B.A. Morrow, J. Phys. Chem. 99 (1995) 14437.
- [51] R. Srinivasan, B.H. Davis, Catal. Lett. 14 (1992) 165.
- [52] J.H. Bitter, K. Seshan, J.A. Lercher, J. Catal. 171 (1997) 279; J.H. Bitter, K. Seshan, J.A. Lercher, J. Catal. 176 (1998) 93; J.H. Bitter, K. Seshan, J.A. Lercher, J. Catal. 183 (1999) 336.
- [53] M. Alfredsson, C.R.A. Catlow, Phys. Chem. Chem. Phys. 3 (2001) 4129.
- [54] H. Zhong, X. Wang, M. Fushimi, A. Endou, M. Kubo, P. Selvam, A. Imamura, A. Miyamoto, Trans. Mater. Res. Soc. Jpn. 29 (2004) 3735.
- [55] J. Boor Jr., Ziegler–Natta Catalysis and Polymerization, Academic Press, New York, 1979.
- [56] R. Martel, A. Rochefort, P.H. McBreen, J. Am. Chem. Soc. 120 (1998) 2421.
- [57] R. Martel, P.H. McBreen, J. Phys. Chem. B 101 (1997) 4966.
- [58] K. Ohe, H. Matsuda, T. Morimoto, S. Ogoshi, N. Chatani, S. Murai, J. Am. Chem. Soc. 116 (1994) 4125.
- [59] M.J.S. Dewar, J. Am. Chem. Soc. 106 (1984) 669.
- [60] W.E. Charles, H.B. Michael, Organometallics 20 (2001) 5606.
- [61] C. Woll, K. Weiss, P.S. Bagus, Chem. Phys. Lett. 332 (2000) 553.
- [62] M.A. Aegerter, M. Jafellicci, D.F. Souza, E.D. Zanotto, Sol–Gel Science and Technology, World Scientific Publishing, Singapore, 1989.
- [63] C.J. Brinker, G.W. Scherer, Sol–Gel Science: The Physics and Chemistry of Sol–Gel Processing, Academic Press, London, 1990.

- [64] E.R. Pohl, F.D. Osterholtz, in: H. Ishida, G. Kumar (Eds.), *Molecular Characterization of Composite Interfaces*, Plenum Press, New York, 1985, p. 157.
- [65] S. Okumoto, N. Fujita, S. Yamabe, *J. Phys. Chem.* 102 (1998) 3991.
- [66] K. Mizushima, P.C. Jones, P.J. Wiseman, J.B. Goodenough, *Mater. Res. Bull.* 15 (1980) 783.
- [67] J.N. Reimers, J.R. Dahn, *J. Electrochem. Soc.* 139 (1992) 2091.
- [68] J.R. Dahn, U. von Sacken, M.W. Juzkow, H. Ai-Janaby, *J. Electrochem. Soc.* 138 (1991) 2207.
- [69] T. Ohzuku, A. Ueda, M. Nagayama, *J. Electrochem. Soc.* 140 (1993) 1862.
- [70] J.R. Dahn, E.W. Fuller, M. Obrovac, U. Sacken, *Solid State Ionics* 69 (1994) 265.
- [71] R.J. Gummow, A. De Kock, M.M. Thackeray, *Solid State Ionics* 69 (1994) 59.
- [72] D.H. Jang, Y.J. Shin, S.M. Oh, *J. Electrochem. Soc.* 143 (1996) 2204.
- [73] K. Suzuki, Y. Oumi, S. Takami, M. Kubo, A. Miyamoto, *Jpn. J. Appl. Phys.* 39 (2000) 4318.
- [74] B. Ammundsen, G.R. Burns, M.S. Islam, H. Kanoh, J. Roziere, *J. Phys. Chem. B* 103 (1999) 5175.
- [75] E. Deiss, A. Wokaun, J.L. Barras, C. Daul, P. Dufek, *J. Electrochem. Soc.* 144 (1997) 3877.
- [76] G. Ceder, Y.M. Chiang, D.R. Sadoway, M.K. Aydinol, Y.I. Jang, B. Huang, *Nature* 392 (1998) 694.
- [77] C. Wolverton, A. Zunger, *Phys. Rev. B* 57 (1998) 2242.
- [78] L. Benco, J. Barras, M. Atanasov, C. Daul, E. Deiss, *J. Solid State Chem.* 145 (1999) 503.
- [79] J.V. Ortiz, R. Hoffmann, *Inorg. Chem.* 24 (1985) 2095.
- [80] M. Meuwly, M. Karplus, *J. Chem. Phys.* 116 (2002) 2572.
- [81] K. Miyata, M. Hori, T. Goto, *Jpn. J. Appl. Phys.* 36 (1997) 5340.
- [82] M. Schaepkens, T.E.F.M. Standaert, N.R. Rueger, P.G.M. Sebel, J.M. Cook, *J. Vac. Sci. Technol. A* 17 (1999) 26.
- [83] K. Takahashi, A. Itoh, T. Nakamura, K. Tachibana, *Thin Solid Films* 374 (2000) 303.
- [84] D. Zhang, M.J. Kushner, *J. Vac. Sci. Technol. A* 19 (2001) 524.
- [85] C.F. Abrams, D.B. Graves, *J. Appl. Phys.* 86 (1999) 5938.
- [86] J. Tanaka, C.F. Abrams, D.B. Graves, *J. Vac. Sci. Technol. A* 18 (2000) 938.
- [87] T. Watanabe, H. Fujiwara, H. Noguchi, T. Hoshino, I. Ohdomari, *Jpn. J. Appl. Phys.* 38 (1999) L366.
- [88] H. Ohta, S. Hamaguchi, *J. Chem. Phys.* 115 (2001) 6679.
- [89] P. Ho, J.E. Jonnannes, R.J. Buss, E. Meeks, *J. Vac. Sci. Technol. A* 19 (2001) 2344.
- [90] P. Waara, J. Hannu, T. Norrby, A. Byheden, *Tribol. Int.* 34 (2001) 547.
- [91] D.E. Weller, J.M. Perez, *Lubr. Eng.* 56 (2000) 39.
- [92] M.Y. Wang, W.F. Feng, *Tribol. Trans.* 40 (1997) 521.
- [93] S.W. Critchley, P. Miles, in: *Proceedings of the Ind. Lubrication Symposium*, Scientific Publishers, Oxford, 1965, p. 21.
- [94] G. McKay, *Chem. Eng. J.* 86 (2002) 343.
- [95] R. Weber, H. Hagenmaier, *Chemosphere* 38 (1988) 529.
- [96] Y. Okamoto, *Chem. Phys. Lett.* 310 (1999) 355.
- [97] Y. Okamoto, M. Tomonari, *J. Phys. Chem. A* 103 (1999) 7686.